The Fortnightly and Monthly Tides: Resonant Rossby Waves or Nearly Equilibrium Gravity Waves?

ARTHUR J. MILLER, DOUGLAS S. LUTHER, AND MYRL C. HENDERSHOTT

Scripps Institution of Oceanography, University of California, San Diego, La Jolla, California

(Manuscript received 2 December 1991, in final form 5 June 1992)

ABSTRACT

The fortnightly and monthly tides are discussed in the light of recent sea level observations and numerical modeling results. Within the tide gauge network of the low-latitude Pacific, the fortnightly tide is shown to possess a large-scale phase lag of roughly 10–40 degrees. Although the nonequilibrium part of the fortnightly tide is traditionally thought to be dominated by Rossby wave dynamics, it is shown, via global shallow-water modeling studies, that this large-scale phase lag is explicable in terms of remotely forced gravity waves whose origin is mainly in the Arctic Ocean. Although future observations outside the low-latitude region of the Pacific may eventually reveal Rossby wave excitation, the fortnightly tidal signal in the tide gauge network at hand appears to reveal at most only weak excitation of Rossby waves compared to the phase lag due to remotely forced gravity waves. The observed monthly tide appears to be only slightly closer to equilibrium than the fortnightly tide. The reason for this remains unclear since the monthly tide is less affected by the remotely forced gravity waves than the fortnightly tide.

1. Introduction

The nature of the oceanic response to long-period tidal forcing has been debated for over two centuries (Laplace 1775; Darwin 1886; Hough 1897; Proudman 1913; Wunsch 1967). The traditional question has been whether or not the long-period tides (LPT hereinafter) are well approximated by their equilibrium forms. The lack of believable observations left turn-of-the-century studies in a purely theoretical state. Wunsch (1967) analyzed observations from Pacific tide gauge stations that showed that the fortnightly and monthly tides are indeed much closer to equilibrium than the diurnal or semidiurnal tides. Since Wunsch modeled the small deviations of these tides from equilibrium in terms of quasigeostrophic dynamics, it has generally been accepted that Rossby wave dynamics explain the dominant part of the nonequilibrium LPT response.

In this paper, we present a different view of the ocean's response to fortnightly tidal forcing. After taking a careful look at new observations (see Figs. 1, 2 and appendix A) and previous numerical modeling results, we arrive at the conclusion that quasigeostrophic dynamics fail to explain the O(1) feature of the observed deviation of the fortnightly tide from equilibrium, roughly a 10–40 degree phase lag in the low-latitude (±30°) Pacific. Our global-scale shallow-water modeling results show that the dynamic portion (i.e., the deviation from equilibrium) of the fortnightly tide observed in the low-latitude Pacific Ocean is not due to Rossby wave dynamics but rather to gravity wave excitation, which can be associated with the Arctic Ocean. This is because the LPT potential projects strongly onto the Arctic Ocean, forcing water out of, or pulling water into, the basin resulting in a gravity wave that propagates into the Pacific Ocean to satisfy global mass conservation. It takes roughly two days for the gravity wave to propagate to the Pacific, with the resultant response in the low-latitude Pacific explaining much of the observed 10–40 degree phase lag.

We emphasize that Rossby/topographic wave excitation is likely to dominate the nonequilibrium response in other regions of the World Ocean, for example, over the East Pacific Rise. But the island tide gauge network at hand does not adequately sample these regions. To set the stage for the numerical modeling results, which ultimately explain the quandary of why quasigeostrophic dynamics fail to account for the observed Mf tide over the present tide gauge network, we give an introduction in the next section of the work since Wunsch's (1967) seminal study. In section 3, we introduce the finite-element time-stepping model of the tides, which we use to obtain solutions in a closed Pacific basin, a near-global ocean, and a global ocean. In section 4, we discuss our results for the fortnightly tide and attempt to relate them to the monthly tide and to the general low-frequency response of the ocean.

2. Historical perspective

Several theoretical models of the LPT have appeared since Wunsch (1967) first suggested that the dynamic

Corresponding author address: Dr. Arthur J. Miller, University of California at San Diego, Scripps Institution of Oceanography, A-024, Climate Research Division, La Jolla, CA 92093-0224.

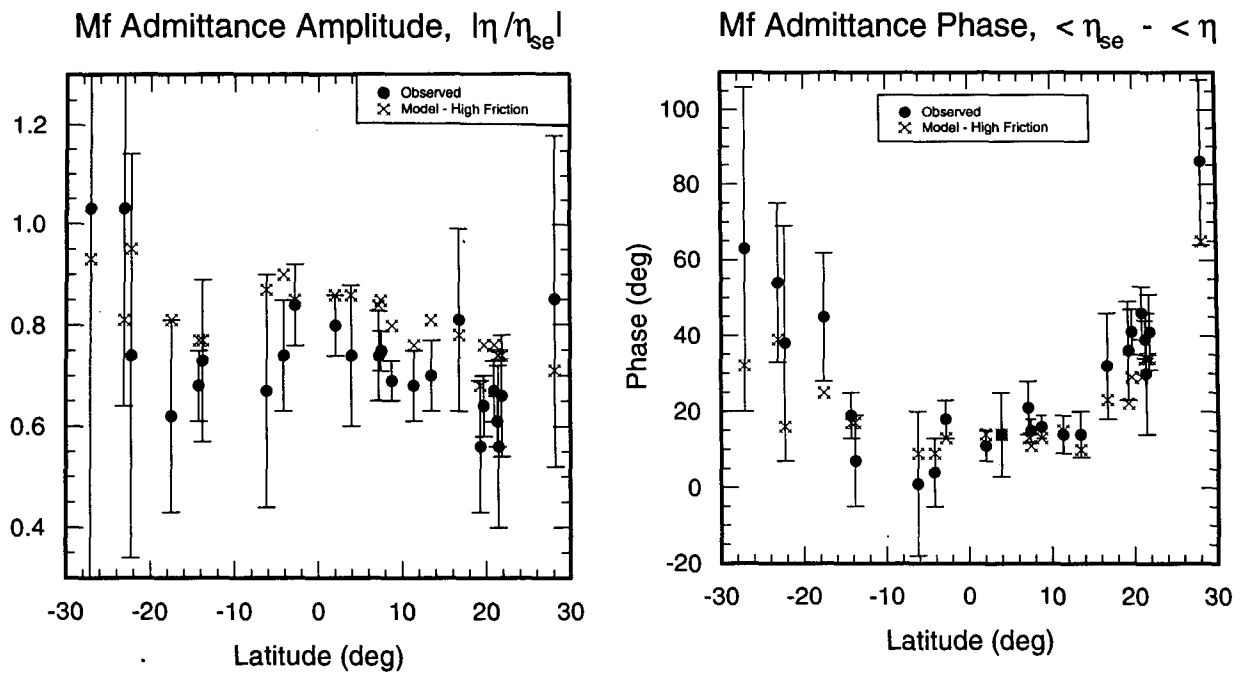

FIG. 1. Admittance (a) amplitude and (b) phase versus latitude for the fortnightly (Mf) tide as estimated from tide gauge records from islands in the low-latitude Pacific Ocean (appendix A). The 90% confidence intervals bracket the spectral estimates. The model values, indicated by x's, are from the global model discussed in the text with 14-day forcing period and $r = 4 \times 10^{-3}/H$ (the high-friction case of Tables 1, 3 and Figs. 8d, 10).

part of the LPT could be understood as a superposition of barotropic Rossby waves excited by the LPT-generating forces in a closed basin. Two distinct interpretations have arisen from these studies: a theoretical small-scale, O(1000 km) wavelength Rossby wavelike response versus a computed basin-scale response which has not been explained. We elaborate on these two views in the following paragraphs.

Wunsch (1967) derived a quasigeostrophic equation for the fortnightly tide and discussed solutions in terms of resonant Rossby modes. Dominant wavelengths in the frequency band of interest were O(1000 km) for his flat-bottom model. The model response exhibited spatial fluctuations and amplitude variations similar to those apparently seen in his data from island tide gauge records in the low-latitude Pacific Ocean (compare Wunsch's Figs. 4–7 with our Figs. 1, 2). We note, as did he, that his solutions, expressed as admittance (η/η_e, where η_e, called the equilibrium tide, is the gravitational forcing expressed as an equivalent sea level displacement), were necessarily displaced by constant values to permit favorable comparison with the observations. Measured admittance phases were generally all positive, while model values had several zero crossings. Measured admittance amplitudes were almost everywhere less than one, while model values were both above and below one, unless friction was introduced. For the frictional case, Wunsch plotted one longitudinal section of model admittance amplitude values that were all less than one. However, that result depends on what latitude is chosen for the section; other latitudes could have admittance values that are uniformly greater than one.

Kagan et al. (1976) integrated Laplace's tidal equations (LTE hereinafter) in a global ocean, with topography, for the fortnightly constituent. They found an "acceptable range" of agreement with Wunsch's observations and described the results, to first approximation, as a superposition of "global-scale oscillations." They concluded that their model response did "not favor" Wunsch's theory of a "superposition of comparatively short Rossby waves." We note that their model employed bottom, as well as Laplacian, friction parameterizations; decay time for the scale-independent, depth-dependent bottom friction was O(50 days). Their grid resolution (5 deg), however, barely resolves the O(1000 km) waves which Wunsch expected to be important.

Agnew and Farrell (1978) recomputed the fortnightly and monthly admittance functions for Wunsch's observations using a static "self-consistent" equilibrium tide (see appendix A). Their computation of the static tide accounted for the yielding of the solid earth (which reduces the equilibrium tide by about 30%), the effects of ocean loading and ocean self-attraction (which increases the previous result by about

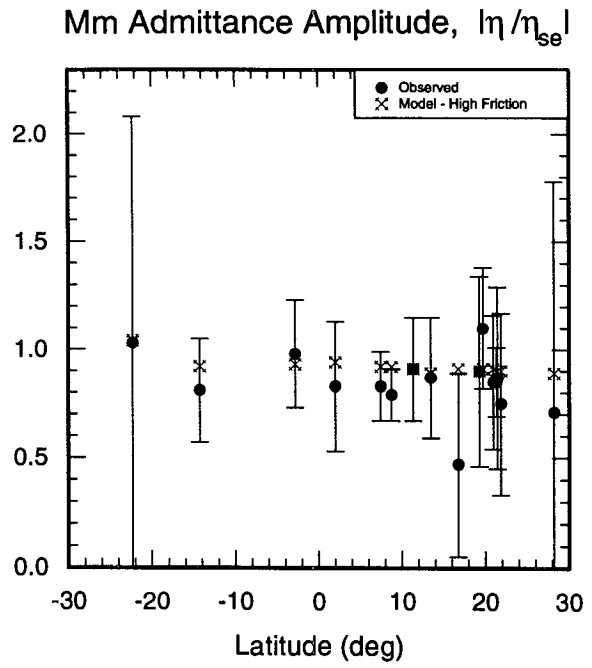

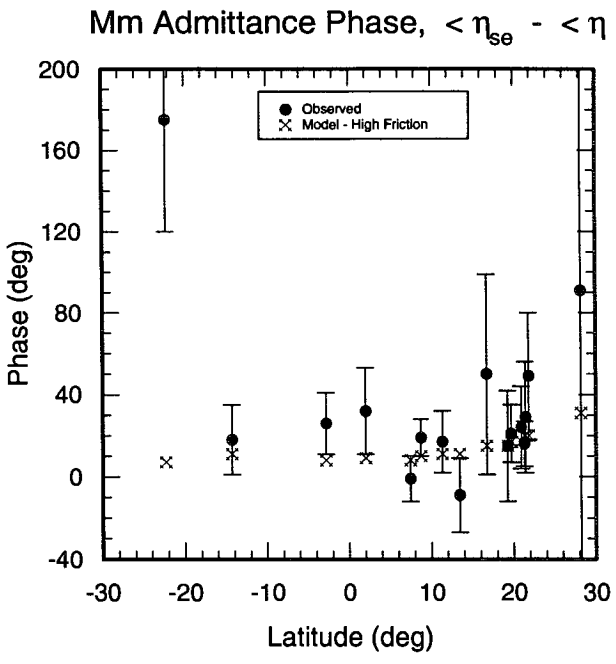

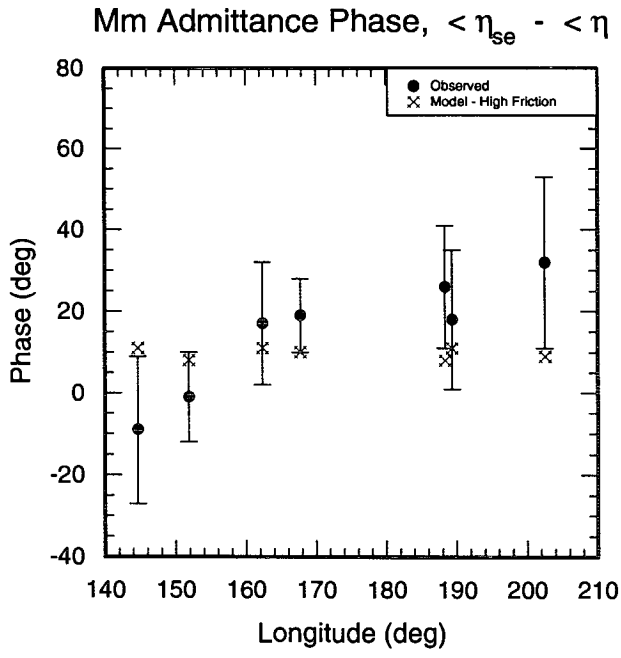

FIG. 2. Admittance (a) amplitude and (b) phase versus latitude for the monthly (Mm) tide, otherwise as in Fig. 1. (c) Admittance phase versus longitude for Mm for stations within 15° of the equator. The model values, indicated by x's, are from the global model discussed in the text with 28-day forcing period and $r = 4 \times 10^{-3}/H$, the high-friction case of Table 3.

25%), and the distribution of the continents (which introduces slight longitudinal dependence and generally reduces the previous result by up to 15%). The observed admittance amplitudes did not change appreciably, although they tended to become closer to one. Admittance phase is not affected by any of the self-consistency effects.

Luther (1980) obtained island tide gauge data from additional stations and with longer records (where overlap occurs) than could Wunsch (1967). He estimated admittance relative to Agnew and Farrell's (1978) self-consistent forcing function, so no arbitrary constant offsets are necessary for comparison with theory. Luther found that there was no significant indication of the O(1000 km) wavelength Rossby wave variations in the admittance, but identified a large-scale deviation of the fortnightly tide from equilibrium as a function of latitude and a slight east–west slope to the

admittance amplitude and phase. The monthly tide variations were much less stable (and were bracketed with larger error bars) than those for the fortnightly tide. The only definitive statement possible was that the size of the variability of the Mm admittance (both amplitude and phase) was comparable to (and perhaps greater than) that of the fortnightly tide.

Schwiderski (1982) integrated LTE in a global domain for both the fortnightly and monthly tides. His model response was also of basin scale, supporting the results of Kagan et al. (1976). However, his "empirical–dynamical" integration scheme both incorporated many observations of doubtful statistical significance and is difficult to interpret dynamically because of the constraints imposed on the solutions by the observations.

Carton (1983) gave a physical argument, based on low-frequency approximations to the shallow-water equations, for observing a westward-intensified response (time-dependent Stommel circulation) that approached equilibrium towards the eastern boundary. His near-global numerical solution of LTE for both fortnightly and monthly forcing (similar to the response to be discussed in Fig. 6) was suggested to substantiate his theoretical prediction. Small-scale fluctuations, consistent with the anticipated weak Rossby wave fluctuations, occurred in the midlatitudes of his near-global (the Arctic was excluded) shallow-water model. Yet there were several regions, particularly the Pacific basin, in which the numerical model deviated from his theory. For example, the topography of the South Pacific basin appeared to produce substantial spatial variability near the eastern boundary. Furthermore, his near-global solution exhibited the large-scale Pacific-wide deviation of the tide from equilibrium to which we are now drawing attention. The model monthly tide was closer to equilibrium as predicted from his highly viscous theory, but this result conflicted with Luther's (1980) interpretation of the observations, as discussed previously, which suggested as strong a deviation from equilibrium as the fortnightly tide.

Dickman (1989) developed a spectral model of the long-period tides based on a spherical harmonic expansion. Considering realistic bathymetry and basin shape, and with bottom friction damping time of 77 days and lateral friction coefficient of 1.5×10^7 $cm^2\ s^{-1}$, Dickman found that the coefficient of the spherical harmonic corresponding to the structure of the equilibrium tide ($l = 2$, $n = 0$) was smaller than the input forcing. This suggests that the large-scale component of the Mf tide approaches equilibrium "from below," which agrees with the low-latitude observations of ~0.8 admittance amplitude; high latitudes of the North Pacific, however, were found to approach equilibrium "from above" in the previously discussed numerical solutions. Since the detailed spatial structure of his solutions was not shown, it is difficult to compare his results with actual oceanic response.

Cartwright and Ray (1990) computed zonal averages of the fortnightly tide admittance as observed from Geosat altimetry observations. These were later reestimated by Ray and Cartwright (1992) and are reproduced here in Fig. 3. The low-latitude component of their results indicates admittance amplitude less than unity and phase lags of order 8 degrees, consistent with Luther's observations. The admittance poleward of about 40 degrees tends to greater (less) than unity in the Northern (Southern) Hemisphere. In their original 1990 analysis, the imaginary component of the zonally averaged admittance exhibited O(1000 km) wavelength variations in the meridional direction (suggesting a Rossby-like wave response); in the reanalysis by Ray and Cartwright (reproduced in Fig. 3), however, the imaginary component has a very smooth response (without these variations). Ray and Cartwright (1992) also show analogous estimates for the monthly tide that show, in line with Luther's (1980) observations, similarly sized deviations from equilibrium although the error bars are much larger for Mm.

In the earlier stages of this work, Miller (1986; chapter 3) reexamined Luther's observations, which had been extended to longer record lengths and supplemented with more stations (Figs. 1, 2 and appendix A), in light of Carton's (1983) numerical results. Miller described a large-scale, low-latitude signal that appears in the fortnightly response of Carton's model and in

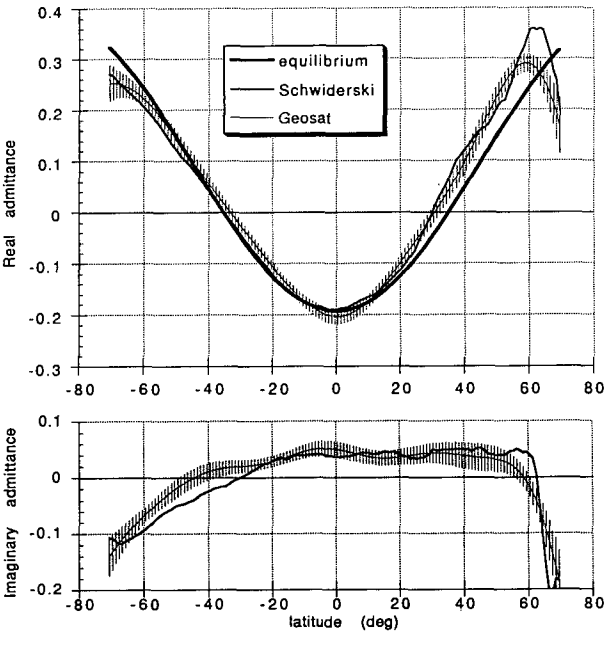

FIG. 3. Real and imaginary parts of the zonally averaged admittance of the satellite-observed fortnightly altimetric tide (thin lines), the analogous tide from the numerical model of Schwiderski (medium line), and the purely real classical equilibrium tide modified to include only loading (thick line), taken from Ray and Cartwright (1992). Vertical lines are 2-σ error bars. The altimetric tide is the sum of the ocean tide and the induced load tide radial displacement.

the observations. As seen in Fig. 1, the large-scale Mf response in the low-latitude (±30°) Pacific has admittance amplitude values of ~0.8 (generally less than 1.0) and admittance phase values of 10–40 degrees (nearly always positive). An analogous low-latitude pattern in monthly admittance amplitude ~0.9 and phase values of 5–15 degrees appears in the numerical models, though it is not as evident in the observations (Fig. 2). After discussing many aspects of quasigeostrophic response to low-frequency forcing, Miller claimed that quasigeostrophic dynamics cannot account for the uniformly positive phase lags seen in Fig. 1 because Rossby wave excitation in the weakly damped case (Wunsch's conceptual model) implies meridional zero crossings in the phase of the response, while strongly damped quasigeostrophic dynamics (Carton's conceptual model) yields admittance amplitudes much too close to unity and very small phase lags, both of which conflict with Fig. 1. If Rossby wave excitation is occurring, it rides upon a large-scale nonquasigeostrophic component of the response. Miller (1986, 1992) attempted to explain this large-scale response by accounting for a divergent velocity field due to nearly equilibrium gravity wave dynamics in a closed Pacific basin, but the result only affected the quasigeostrophic portion of the total response.

In summary, Figs. 1 and 2 stand in contrast to the limited set of Mf and Mm observations described by Wunsch (1967) as containing short-scale variations associated with Rossby wave activity. Our new long-period tidal observations instead substantiate the large-scale, low-latitude responses, which occur in the published numerical models of the fortnightly tide. Rather than exhibiting Rossby wave–scale variations, Fig. 1 shows that the Mf admittance amplitude and phase bear an interesting bow-shaped structure, nearly symmetric about the equator. Figure 2 shows that, although the Mm admittance amplitude is closer to unity than is that of the Mf, the Mm admittance phases are nearly as large as those for Mf and are typically larger than the numerical models predict.

The most obvious questions that arise from this historical perspective are then: What is the mechanism that generates the large-scale, low-latitude response in the Pacific fortnightly tide? Does the Mm tide deviate as much from equilibrium as does the Mf, and if so, why? In the next section, we show that the answer to the first question is contained in the Arctic Ocean. Some speculation on the second question is given in the discussion section.

3. Shallow-water models of the fortnightly tide

To divest ourselves from any quasigeostrophic restrictions, we now examine some linear shallow-water models of the long-period tides. We solve LTE (Lamb 1932, chapter 8; Miles 1974; Hendershott 1981), namely,

$$\frac{\partial u}{\partial t} - 2\Omega \sin\theta v = -\frac{\partial}{\partial \phi}(\eta - \Gamma/g)/a\cos\theta - ru, \tag{3.1a}$$

$$\frac{\partial v}{\partial t} + 2\Omega \sin\theta u = -\frac{\partial}{\partial \theta}(\eta - \Gamma/g) - rv, \tag{3.1b}$$

$$\frac{\partial \eta}{\partial t} + \frac{1}{a\cos\theta}\left[\frac{\partial}{\partial \phi}(uH) + \frac{\partial}{\partial \theta}(vH\cos\theta)\right] = 0, \tag{3.1c}$$

in standard notation, on the sphere for various basin geometries, topographies, and frictional parameterizations. The boundary condition of no flow through the boundary is upheld for all boundaries in each geometry considered.

We use a finite-element model (appendix B and Fig. 4a), with LPT forcing (Fig. 4b) and linear bottom drag ($r = \epsilon/H^n$, where ϵ is a constant, H is the depth, and n is an integer). Our basic, or normal, choice for friction is $r = 10^{-3}/H$, which corresponds to the bottom drag

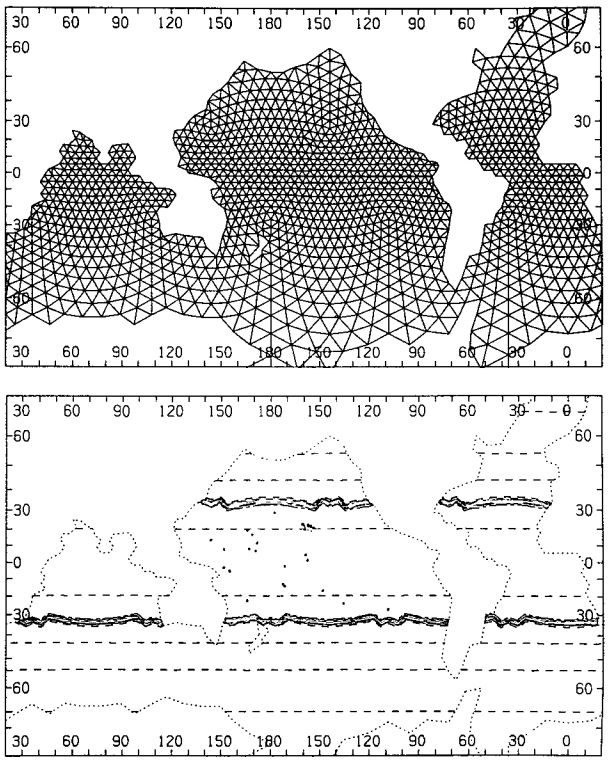

FIG. 4. (a) The finite-element resolution for the global model. The average area of a finite-element triangle is equal to the area of a 3.1° equatorial square. The islands of Antarctica, New Zealand, and Hawaii are included in the global and the near-global geometry. Hawaii is not included in the closed-Pacific case. The topography is taken from the Rand/SIO 1° observations. (b) The equilibrium tidal forcing function used in the global model. The amplitude at the Pacific equator is 1.28 cm. The nodal lines of the P_{20} spherical harmonic are indicated by the clustering of phase near 35N and 35S. The mean is removed for all cases. The dots indicate the approximate locations of the island tide gauge stations discussed in the text and Figs. 1 and 2.

law used by Kagan et al. (1976). For a 4000-m constant depth ocean, this frictional choice implies an exponential damping time scale of 46 days. Many other numerical experiments were run with different values of ϵ and n, though only a few are discussed here. The equilibrium tide, to which we reference solutions, always includes the proper mass conservation constant for that particular solution's geometry.

We first consider a closed Pacific basin to determine the extent to which the local response to the tidal potential in the Pacific by itself can explain the large-scale deviation of the fortnightly tide from equilibrium. Figure 5 shows the phase of the observable tide, the admittance amplitude, and the dynamic tide ($\eta - \eta_e$) for 14-day forcing and $r = 10^{-3}/H$. One can see from the admittance amplitude (Fig. 5b) that the low-latitude Pacific is very close to equilibrium in this case. The phase lag in the low latitudes, though tending to have large spatial scale and a slight slope across the basin (Luther 1980), is only a few degrees (Table 1; Fig. 5a). As can be seen from the dynamic tide (Fig. 5c,d), although there is substantial Rossby wave excitation in the vicinity of the East Pacific Rise and to a lesser extent near the forcing nodal line of the North Pacific, there is little excitation of Rossby waves in the low latitudes. Though not so evident in this figure, the region between Fiji and the East Pacific Rise (170–120W), which is relatively flat, is a locale that, for lower friction cases with higher resolution, supports the clearest signal of Rossby wave–like excitation in the Pacific.

Although we present only one case for the closed Pacific geometry, we emphasize that we have run many different versions of this case (differing frictional amplitudes and forms, different basin shapes, topographies, and resolutions), but we failed to find a parameter that clearly controls the size of the phase lag in the low-latitude Pacific Ocean.

Since Carton's (1983) near-global shallow-water model did show a stronger phase lag and admittance amplitudes further from unity than our closed-Pacific cases (see Table 1), we attempted to reproduce Carton's results with a near-global model (Fig. 6), which omits only the Arctic Ocean. As can be seen in Table 1 and to some extent in Fig. 6a, the phase lag in the low-latitude Pacific of the near-global ocean is increased over the closed Pacific case and more closely resembles Carton's results. The differences in admittance amplitude between Fig. 6b and Carton's results (his Fig. 8a) probably stem from Carton's using Agnew and Farrell's (1978) self-consistent tide as forcing, which conserves mass for the global ocean, but not necessarily for the near-global ocean model of Carton. Indeed, a small

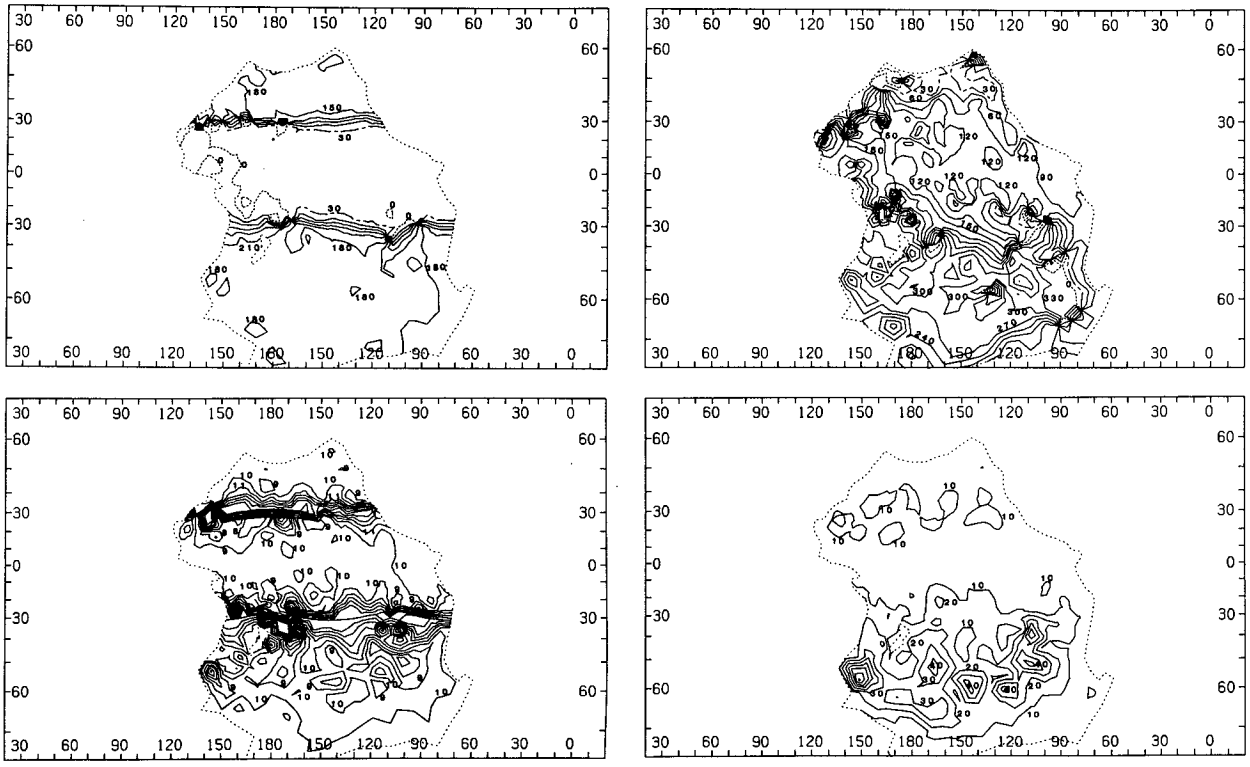

FIG. 5. Closed Pacific Ocean case with $r = 10^{-3}/H$ (normal friction). (a) Phase of the model Mf tide (contour interval: 30°). Zero phase is indicated by the dotted line and 30° phase is indicated by the long dashed line. (b) Admittance amplitude of the model Mf tide (CI: 0.1, contours scaled by 10). (c) Phase of the model Mf dynamic tide (CI: 30°), otherwise as in (a). (d) Amplitude of the model Mf dynamic tide (CI: 10, contours scaled by 63.6 cm).

TABLE 1. Phase (deg) of Mf tide at selected locations.

Location	Observed	Carton (1983) near-global	Closed Pacific basin	Near-global (no Arctic)	Global (with Arctic)	High-friction global (with Arctic)
Midway	86	74	−22	11	32	65
Nawiliwili	41	26	8	19	29	34
Mokuoloe	30	25	8	19	29	34
Honolulu	39	25	8	19	29	34
Kahului	46	26	8	17	25	29
Hilo	41	30	8	17	25	29
Wake	36	28	13	19	26	22
Johnston	32	12	4	8	18	23
Guam	14	3	−3	3	7	10
Eniwetok	14	8	7	11	16	15
Kwajalein	16	12	7	11	16	13
Truk	15	7	−2	4	8	11
Majuro	21	14	2	7	12	13
Fanning	14	10	3	8	12	14
Christmas	11	10	3	7	12	14
Canton	18	11	3	8	13	13
Rabaul	4	6	−3	3	7	9
Anewa Bay	1	8	0	5	10	9
Apia	7	7	6	9	16	17
Pago Pago	19	8	6	9	16	17
Papeete	45	21	10	19	24	25
Noumea	38	12	5	14	19	16
Rikitea	54	23	23	34	45	39
Easter	63	40	0	10	25	32

The closed-Pacific, near-global, and global models have $r = 1 \times 10^{-3}/H$ frictional parameterization. The high-friction global model has $r = 4 \times 10^{-3}/H$.

constant added to our (mass-conserving) equilibrium tide causes Fig. 6b to bear admittance amplitude structure very similar to Carton's Fig. 8a. Further differences between our results and Carton's probably arise from differences in resolution, the Laplacian frictional parameterization used by Carton, or the number of tidal cycles integrated.

Since the admittance phase does not change by adding a constant to the equilibrium tide, a dynamic effect must cause the large-scale phase lag in the low-latitude Pacific. We therefore hypothesized that gravity waves excited in remote basins must travel to the Pacific (to satisfy mass conservation in the near-global ocean) with finite phase speeds, resulting in the observed phase lags in the Pacific. In particular, the strong projection of the Mf tidal potential onto the Arctic might provide the key to controlling the size of the phase lag in the Pacific. We therefore included the Arctic in a global model of the Mf tide and indeed found (Fig. 7; Table 1) an even stronger low-latitude Pacific phase lag than for the near-global geometry, in line with our hypothesis. Figure 8 shows a close-up view of the Mf phase lag in the low-latitude Pacific showing that as the geometry increases from Pacific-basin scale to global scale the phase lag increases as well. (The effect of friction on the phase lag is discussed below.)

To further clarify the remotely forced response in the Pacific, we ran several more cases in which we set the tidal forcing function to zero everywhere except north of the nodal line in the North Atlantic and Arctic Oceans, that is, a tidal forcing mechanism localized in the Arctic. We ran this case both with a flat bottom and with oceanic topography for similar friction parameters as in the global model (the dynamic tide for one case is shown in Fig. 9). The observable tide in the Pacific lags the equilibrium by about 60 degrees (2.3 days). The amplitude of the dynamic tide in these cases is typically at least as large as, and often larger than, the dynamic tide from the closed Pacific cases (Table 2; Figs. 5c,d; 6c,d; 7c,d; 9a,b), and the phase of the dynamic tide was likewise comparable to results with the total equilibrium tide as forcing. This result supports our claim that waves traveling out of the Arctic Ocean contribute significantly to the observable Mf tide in the low-latitude Pacific.

It remained to be determined if gravity waves or Rossby waves were being excited by the Arctic forcing. Intuitively, one expects that Rossby waves would be less important since the time scale of energy propagation would probably be much longer than for the gravity waves, but it is difficult to estimate the propagation time scale when considering the anisotropic group velocity of Rossby waves and the added complication of the irregular topography of the oceans.

We therefore ran two test cases, one with gravity reduced by a factor of 2, and one with the rotation rate

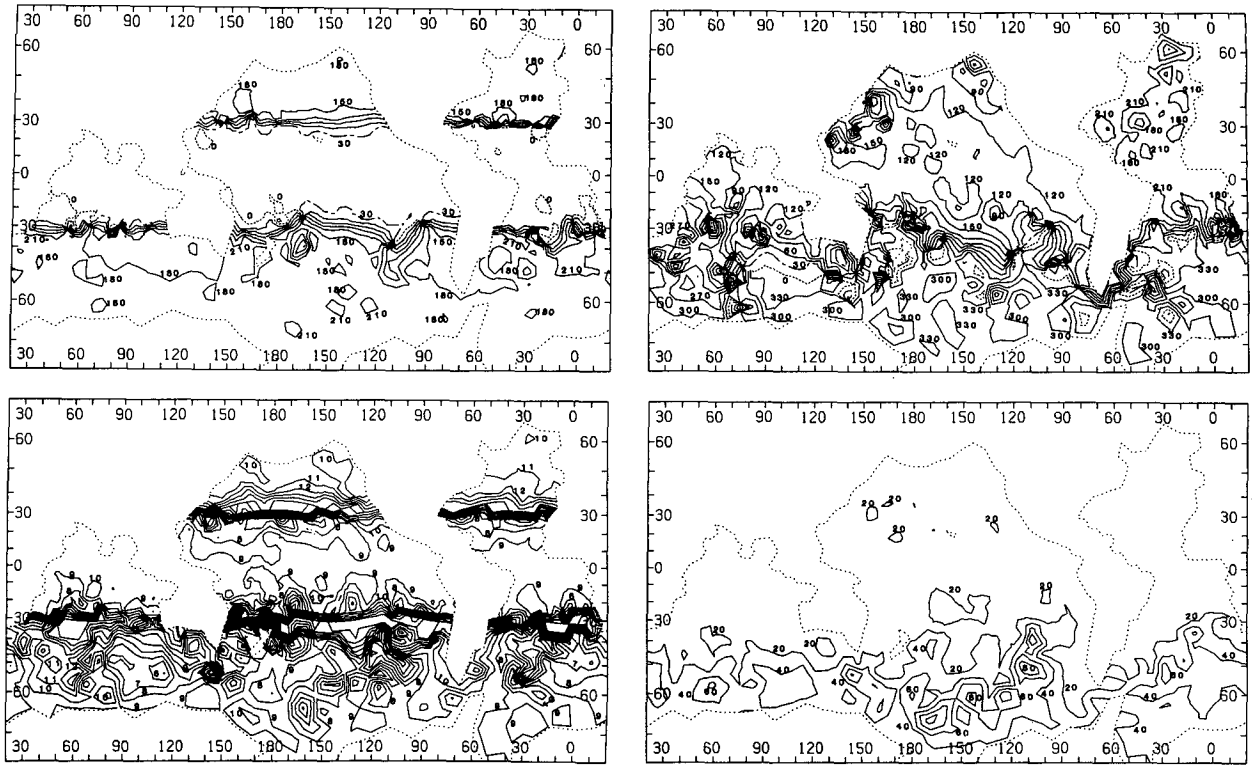

FIG. 6. Near-global case with $r = 10^{-3}/H$ (normal friction). (a) As in Fig. 5a. (b) As in Fig. 5b. (c) As in Fig. 5c. (d) As in Fig. 5d but CI: 20.

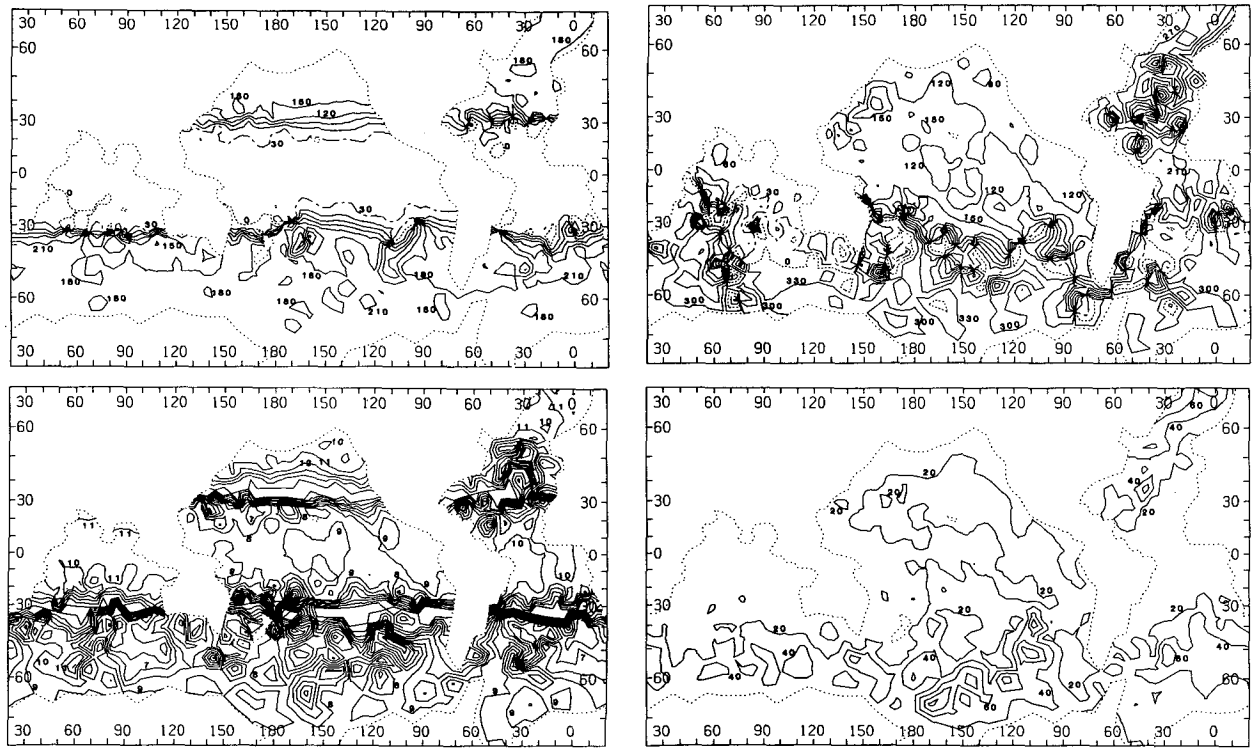

FIG. 7. Global case with $r = 10^{-3}/H$ (normal friction). (a) As in Fig. 5a. (b) As in Fig. 5b. (c) As in Fig. 5c. (d) As in Fig. 5d but CI: 20.

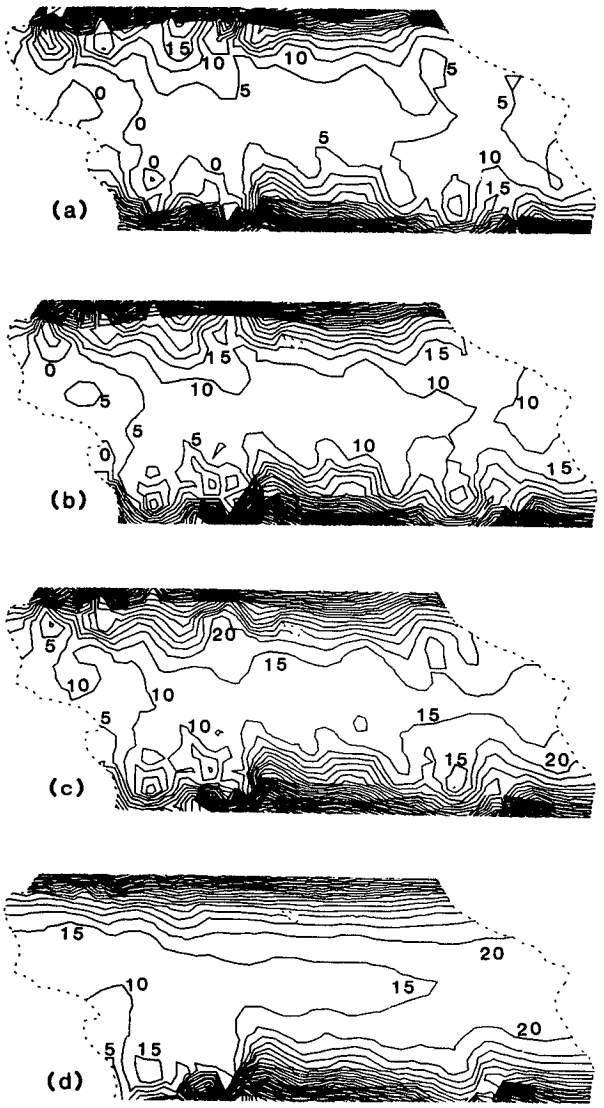

FIG. 8. Expanded views of the low-latitude (±30°) Pacific Ocean phase lag of model fortnightly tides, with contour intervals of 5 deg. (a) Analogous to Fig. 5b (closed Pacific with normal friction). (b) Analogous to Fig. 6b (near-global with normal friction). (c) Analogous to Fig. 7b (global with normal friction). (d) Analogous to Fig. 10b (global with high friction).

reduced by a factor of 2, both with Arctic forcing only. For the first case, one would expect that if gravity (e.g., Kelvin) waves were responsible for the Pacific response, the phase lag of the observable tide would be increased. This is indeed the case, with phase lags corresponding to roughly $\sqrt{2}$ times the normal case, in accord with the dispersion relation for gravity (e.g., Kelvin) waves. For the second case, the slower rotation reduces the amplitude of both the β effect and of the vorticity perturbation produced by topographically induced stretching of planetary vorticity, both of which would reduce the speed of groups of short Rossby waves, resulting in a larger phase lag if this mechanism is important. In other words, an inspection of the barotropic vorticity equation clearly shows that the wave frequency scales with the rotation rate and β, regardless of the choice of topography. For the reduced rotation case, however, instead of an increase in lag, we found that the phase lag in the Pacific decreased 40%–50%. This again suggests that gravity waves, influenced by rotation, explain the phase delay, since rotation can slow gravity waves both by directly affecting the dispersion relation and/or by forcing the gravity wave to follow circuitous coastally or equatorially trapped routes in the form of Kelvin-like waves. Thus, the phase lag in the Pacific is clearly due to gravity wave effects.

What route does the gravity wave take to reach the Pacific from the Arctic? Clearly, the wave must propagate south through the Atlantic Ocean and then either through the Drake Passage or through the Indian Ocean (or through both) to the equatorial Pacific (Fig. 9b). We anticipate that the gravity wave will follow coastlines and equatorial zones from Arctic to Pacific in the same sense as Kelvin waves, since rotation causes gravity waves at long periods to be biased towards boundary or equatorial trapping in the form of Kelvin-like waves. By inspecting the phase distribution for the global case with normal friction and global LPT forcing (in maps with better detail than Fig. 7), we find that the low-latitude Atlantic Ocean leads the equilibrium by about 5 degrees, the low-latitude Indian Ocean lags by about

TABLE 2. Amplitude (cm)/phase (deg) of model Mf dynamic tide at selected locations.

Location	Closed Pacific basin	Near-global (no Arctic)	Global (with Arctic)	Global Arctic forcing only
Midway	.15/191	.23/176	.25/155	.13/137
Nawiliwili	.10/133	.22/138	.33/128	.13/115
Mokuoloe	.10/133	.22/138	.33/128	.13/115
Honolulu	.10/133	.22/138	.33/128	.13/115
Kahului	.10/133	.23/136	.34/126	.13/116
Hilo	.10/128	.23/136	.34/126	.13/116
Wake	.21/141	.32/144	.44/143	.14/135
Johnston	.10/152	.17/150	.30/137	.11/124
Guam	.11/207	.18/167	.22/150	.09/124
Eniwetok	.18/150	.27/147	.37/143	.12/136
Kwajalein	.15/130	.25/137	.37/134	.14/133
Truk	.08/211	.14/154	.22/138	.10/114
Majuro	.05/137	.17/136	.27/126	.12/117
Fanning	.06/111	.17/121	.28/121	.13/124
Christmas	.06/103	.17/121	.28/119	.13/122
Canton	.06/114	.19/127	.30/122	.12/120
Rabaul	.07/244	.10/154	.17/130	.09/107
Anewa Bay	.05/181	.15/139	.24/128	.11/120
Apia	.12/140	.24/147	.35/138	.14/126
Pago Pago	.12/140	.24/147	.35/138	.14/126
Papeete	.12/86	.26/99	.35/112	.12/120
Noumea	.05/73	.16/85	.24/98	.10/133
Rikitea	.22/85	.32/110	.50/113	.15/123
Easter	.00/68	.06/102	.18/123	.15/123

Each model has $r = 1 \times 10^{-3}/H$ frictional parameterization.

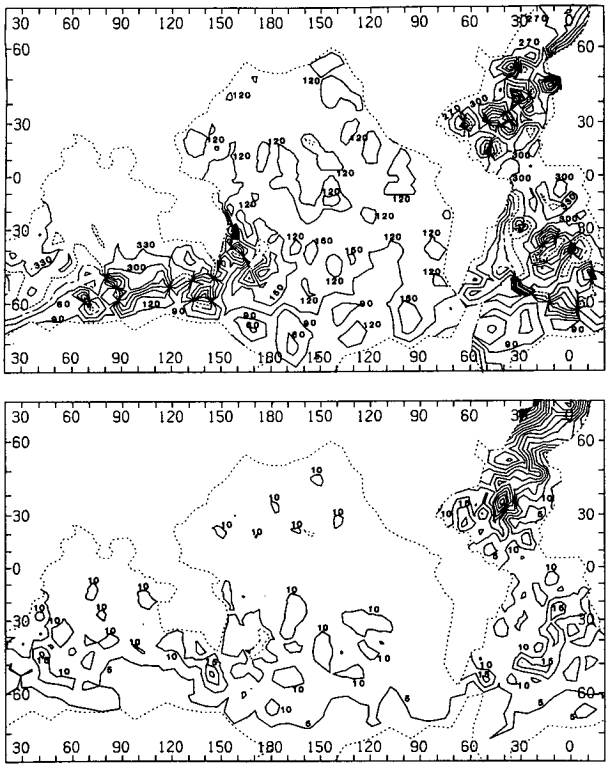

FIG. 9. Arctic-forced case. Same topography, geometry, and friction as for global case in Fig. 7 but tidal potential is set to zero everywhere but north of the nodal line in the North Atlantic. (a) As in Fig. 5c. (b) As in Fig. 5d but CI: 5.

5 degrees while the low-latitude Pacific Ocean lags by about 15 degrees. This result, combined with the longer distance from the Arctic to the Pacific through the Indian Ocean suggests that the Indian Ocean route is followed; a 30 000-km (270°) route with 3000-m effective ocean depth (170 m s^{-1} gravity wave group velocity) implies roughly a 2.0-day Pacific Mf phase lag, consistent with the observed 2.3-day lag. However, if the gravity, or Kelvin-like, wave response is significantly affected by shallower waters, it will then travel much more slowly and may take a more direct route to the tropical Pacific.

We lastly address what effect the strength of friction has on the admittance phase lag and admittance amplitude in the Pacific. We ran the global geometry case for one-half, two times, four times, and eight times the dissipation strength in the normal friction case of Fig. 7. For a 4000-m constant depth ocean, these choices for friction imply exponential damping time scales of 92, 23, 12, and 6 days, respectively. We indeed found a dependence of the admittance phase and amplitude on the strength of friction. As the strength of friction was increased for the fortnightly tide, we found somewhat larger phase lags and lower admittance amplitudes occurred in the low-latitude Pacific (Tables 1, 3; Fig. 10), up to the point of the eight-times normal friction case where the admittance started to edge back towards equilibrium. This result suggests that friction slows the group velocity of the barotropic gravity waves emanating from the Arctic (e.g., Mofjeld 1980; Davey et al. 1983). For the fortnightly tide, as friction is reduced, we found that, although much larger planetary-topographic wave activity occurred in many parts of the basin, in the low-latitude Pacific the response surprisingly tended to move closer to equilibrium. For the monthly tide, a similar test of the strength of friction was less conclusive (Table 3). Admittance amplitude tended towards equilibrium for larger friction, while admittance phase tended to increase slightly with friction. Higher resolution will be required to properly account for the behavior of the monthly tide.

4. Discussion

We have shown that a dominant part of the low-latitude response of the Pacific Ocean to the fortnightly tidal forcing is due to a gravity wave excitation mechanism whose principal source is in the Arctic Ocean. The time scale of propagation from the Arctic to the Pacific is about 2.3 days. The sum of the local dynamic response (e.g., Figs. 5c,d) and the remotely driven dynamic response (e.g., Figs. 9a,b) yields a ~10–40 de-

TABLE 3. Admittance amplitude/phase (deg) of model Mf and Mm tides at selected locations.

	Mf		Mm	
Location	normal friction	high friction	normal friction	high friction
Midway	.50/32	.71/65	.78/22	.89/31
Nawiliwili	.80/29	.74/34	.92/19	.90/20
Mokuoloe	.80/29	.74/34	.92/19	.90/20
Honolulu	.80/29	.74/34	.92/19	.90/20
Kahului	.82/25	.76/29	.93/16	.91/17
Hilo	.82/25	.76/29	.93/16	.91/17
Wake	.68/26	.68/22	.84/14	.90/15
Johnston	.78/18	.78/23	.92/17	.91/15
Guam	.83/7	.81/10	.85/11	.89/11
Eniwetok	.75/16	.76/15	.86/10	.91/11
Kwajalein	.81/16	.80/13	.88/10	.92/10
Truk	.87/8	.85/11	.88/7	.92/8
Majuro	.89/12	.84/13	.91/7	.93/9
Fanning	.91/12	.86/14	.91/8	.93/9
Christmas	.91/12	.86/14	.92/8	.94/9
Canton	.90/13	.85/13	.92/7	.93/8
Rabaul	.92/7	.90/9	.93/5	.95/6
Anewa Bay	.90/10	.87/9	.94/6	.94/7
Apia	.79/16	.77/17	.92/11	.92/11
Pago Pago	.79/16	.77/17	.92/11	.92/11
Papeete	.93/24	.81/25	.91/11	.92/15
Noumea	1.01/19	.95/16	1.10/12	1.04/7
Rikitea	.99/45	.81/39	.85/13	.88/19
Easter	.84/25	.93/32	.89/12	.93/18

Each model has global geometry. Normal friction has $r = 1 \times 10^{-3}/H$. High friction has $r = 4 \times 10^{-3}/H$.

gree phase lag of the observable tide with respect to the equilibrium tide. Thus, we have explained a puzzling aspect (the phase lag) of the discrepancy between quasigeostrophic theories of the fortnightly tide and Pacific observations. The main effects that control the phase lag in the Pacific are the extent to which the tidal potential projects onto remote basins (in particular, the Arctic Ocean is strongly forced by the tidal potential) and the resulting *dynamic* effect of the conservation of mass requirement for the global equilibrium tide (i.e., gravity wave excitation). On the global scale, friction can surprisingly push the Mf tide further from equilibrium by slowing the circumglobal propagation of these gravity waves.

It therefore has become clear why the admittance amplitude is less than unity in the low-latitude Pacific, since the vector sum of the equilibrium tide (zero phase, unit amplitude) and the dynamic tide due to nearly equilibrium gravity waves (120 deg phase with 0.1 amplitude) implies admittance amplitude somewhat less than one and admittance phase of O(10 deg). However, it is also clear that the admittance amplitude is sensitive to the precise calculation of the mass conservation constant of the equilibrium tide, and this sensitivity can probably explain much of the remaining discrepancy between models and observations (Figs. 1, 2, 7, 10). The disturbing feature of the admittance amplitude's dependency on the self-consistency of the equilibrium tide is that it can give the impression of a substantial deviation from equilibrium in the basin of interest, when actually it could be indicating simply mass conservation with no dynamics. For example, consider two connected basins of equal area, for one of which the equilibrium tide has zero mean and for the other of which the equilibrium tide has a large mean value. If we study the first basin in isolation and find a dynamic tide, the dynamic response is meaningful. If we consider the two basins together, however, the local dynamic response in the first basin will be tainted, and perhaps swamped, by the constant for mass conservation (even without considering gravity wave propagation). Of course, the velocity field for the first basin is virtually the same in either approach, but to speak of a dynamic tide in the latter case is inaccurate and confuses the issue of "equilibrium."

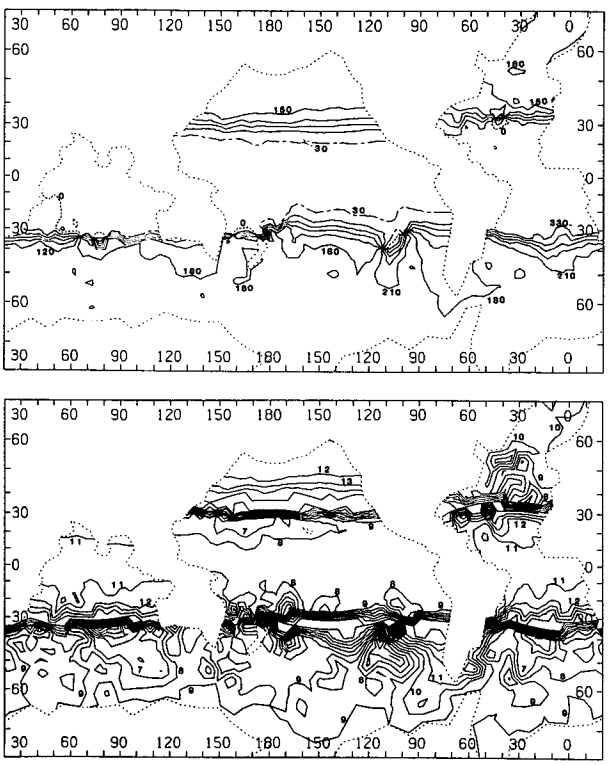

FIG. 10. Global case with $r = 4 \times 10^{-3}/H$ (high friction). (a) As in Fig. 5a. (b) As in Fig. 5b.

Although we suggest that low-latitude Pacific sea level observations of the fortnightly tide are significantly influenced by gravity wave processes, we are not claiming that quasigeostrophic response is unimportant for the fortnightly tide (examine the middle and high latitudes in Figs. 5d, 6d, and 7d). But to properly ascertain the importance of Rossby wave dynamics, the dynamic effect of water sloshing back and forth between the basins must first be identified and removed before the local planetary–topographic resonances can be identified.

A final point of comparison with observations lies in the satellite observations of Cartwright and Ray (1990) and Ray and Cartwright (1992) from which they computed the zonally averaged response of the fortnightly and monthly altimetric tides. An interesting feature of their satellite-observed Mf response, which is reproduced here in Fig. 3, is that it lines up more closely to their theoretically determined classical equilibrium tide (shown in Fig. 3) than to their self-consistent equilibrium tide (not shown). We have computed the analogous Mf response for our various model runs, one of which is shown in Fig. 11. The large-scale structure of our model Mf tide is similar to the satellite-observed Mf structure (as is Schwiderski's model result in Fig. 3), particularly in the latitudinal asymmetry with respect to our mass-conserving equilibrium tide. Although the low-latitude structure is not very sensitive to changes in the strength of friction, for cases with weaker friction the global model predicts a maximum, near 75°N, in the real part of the admittance, similar to that seen in Fig. 3, and the imaginary part tends to become more strongly negative in the Arctic. For stronger friction, the real part of the admittance north of about 50°N drops below the equilibrium. Analogous plots for our model monthly tide (not shown) are rather similar to Fig. 11, although they tend to be closer to equilibrium. In contrast, the satellite-observed monthly tide (see Ray and Cartwright 1992) exhibits deviations from equilibrium that are as large as those for Mf, though the error bars prohibit conclusive statements.

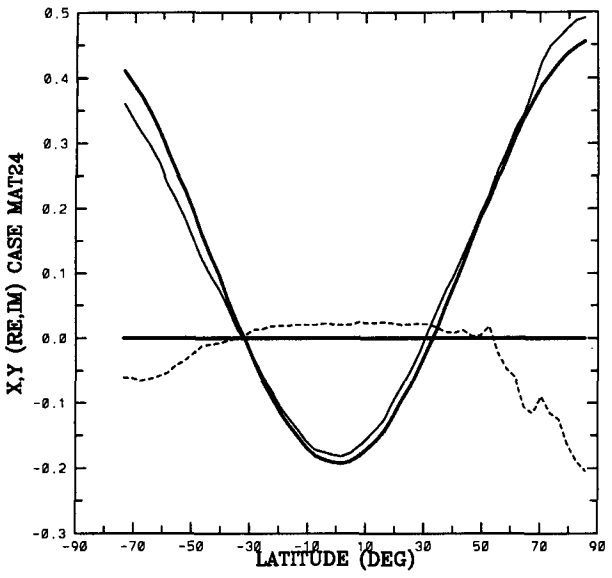

FIG. 11. As in Fig. 3 but for the normal friction global model Mf tide of Fig. 7, following the plotting conventions of Cartwright and Ray (1990) and Ray and Cartwright (1992). The real part of the Mf model tide (thin solid line) bears a fairly similar relation to the model self-consistent equilibrium tide (thick solid line) as does the satellite-observed structure. The imaginary part of the Mf model tide (thin dashed line) also has large-scale structure comparable to the satellite observations.

It is interesting to note that although Rossby wavelike structures do appear in our model solution, they are extinguished in Fig. 11 by the zonal integral, even for cases with much weaker friction. Thus one should not expect zonal mean satellite observations of sea level to exhibit evidence for Rossby wave excitation. For a feel of how strongly Rossby waves are excited, the globally averaged rotational kinetic energy averaged over a tidal cycle increased by 68% for a weak friction case, with constant $r = (100 \text{ days})^{-1}$, over the standard case (irrotational kinetic energy is insignificant); the ratio of kinetic to potential energies was 7.7 in the weak friction case, compared to 5 for the standard case.

Returning to the question of why the monthly tide appears to be nearly as far from equilibrium as the fortnightly, we speculate the following. The phase lag for the monthly tide due to the Arctic-forced response in the Pacific is less than that of the fortnightly, simply because of the disparate frequencies. So, if neither tide was resonant locally in the low-latitude Pacific, the monthly tide would be closer to equilibrium than the fortnightly as theory would suggest. This partially explains the monthly tide's admittance amplitude and phase structure (Fig. 2). However, although we have seen that there is scant excitation of Rossby waves in the low-latitude Pacific for moderate friction values and 14-day forcing, it may be fortuitous that at 28-day periods planetary-topographic waves are more prevalent. Thus, although the fortnightly tide appears to be strongly influenced by the effect of the Arctic, the monthly tide may be more influenced by local Rossby-like oscillations. We note that, although we have run and examined several cases with 28-day period forcing (Fig. 2 shows some results extracted from a run with high friction), our numerical model probably does not have sufficient resolution to properly model these monthly period waves, so we leave the resolution of this problem to future modeling efforts.

Of what consequence are these results to other low-frequency problems in dynamical oceanography? Clearly, if global-scale atmospheric pressure has sufficiently large imbalances from basin to basin [see Ponte et al. (1991), and Davis and Bogden (1989), for evidence that this may indeed be the case], there will be a similar gravity wave adjustment which can lead to remotely forced responses from basin to basin. If one then measures, say, bottom pressure or sea level variations (with 1–20-day periods) in one basin and attempts to model the response as being driven solely by local or basin-scale forcing by wind or atmospheric pressure, then there will likely be discrepancies between the observations and the locally modeled response due to waves excited by the global imbalances of atmospheric pressure. It is doubtful that the remotely driven response in sea level can have sufficiently small scales (horizontal gradients) to be associated with significant current fields but this effect should be examined further.

Acknowledgments. Financial support was provided by NSF Grant OCE88-00080, NOAA Grant NA90-AA-D-CP526, NASA Grant NAG5-236, the G. Unger Vetlesen Foundation, and the University of California INCOR Program for Global Climate Change. AJM completed parts of this work while an Orsen Anderson Visiting Scholar at the Institute of Geophysics and Planetary Physics at the Los Alamos National Laboratories. George Platzman generously provided his normal-mode codes which were both used in unaltered form and converted into the dissipative time-stepping model. Duncan Agnew and Jim Carton provided us with numerical data from their model results. AJM greatly appreciates the many conversations he had with George Platzman, Mark Swenson, Janet Becker, Annalisa Griffa, John Miles, and Phil Bogden. Comments on the manuscript by David Cartwright, Boris Kagan, and the two helpful referees are gratefully appreciated.

APPENDIX A

Tide Estimation

Tide gauge records from the Pacific were obtained primarily from the National Ocean Service and the TOGA Sea Level Center at the University of Hawaii. While data have been obtained for continental coastal stations, this first analysis concentrates on only the tropical island stations that have lower background "noise" levels than the coastal stations, and therefore

have provided the greatest reliability in the tidal estimates. North of the equator, the island stations range from 144°E to 155°W, while south of the equator they range from 152°E to 109°W (Table A1).

All records were originally at least hourly samples rounded to the nearest 0.1 foot, with some records rounded to the nearest 0.1 cm. Errors due to this "least count" roundoff and errors due to instrumental frequency response characteristics and drift are quite negligible at the fortnightly and monthly periods of interest.

The data were subjectively scanned for obvious "bad" points and gaps. Single "bad" points and gaps up to 48 h were filled by linear interpolation of neighboring values. Larger gaps were not filled, but rather just flagged and subsequently avoided. Errors in the time axis of each record were sought by examination of the phase of the complex-demodulated M_2 tide. Phase jumps were not uncommonly found to be due to incorrect times following a change in a station's time zone relative to GMT, that is, an hour was incorrectly added or dropped from a record.

Surface air pressure data was obtained from the National Climate Data Center, where overlap with existing sea level data occurred. The air pressure was examined and edited in a manner similar to the sea level data. Sea level was then "adjusted" for the isostatic effect of air pressure fluctuations by adding $P_{air}/\rho g$ to the sea level data, where the mean sea surface density ρ at each station was approximated from Levitus (1982). A list is given in Table A1 of the "adjusted" and "unadjusted" sea level data used to estimate the fortnightly and monthly tides. To obtain tide estimates the data were fast Fourier transformed (FFT), with no data tapering prior to transformation. Further details of the estimation procedure are provided later.

A sea level fluctuation that has an amplitude and phase corresponding exactly to that predicted from the amplitude and phase of the moon's and/or sun's gravitational forcing is called an equilibrium tide η_e. The form of the equilibrium tide in the ocean for the long-period fluctuations of gravity (excluding oceanic self-attraction and deflection of the surface of the solid

TABLE A1. Sea level stations.

Station	Latitude	Longitude	Total number of years of data	Sea level years	
				Unadjusted	Adjusted
Midway	28°13'N	177°22'W	19	0	1950–1958 1960–1971
Nawiliwili	21°57'N	159°22'W	18	0	1954–1972
Mokuoloe	21°26'N	157°47'W	13	0	1957–1969
Honolulu	21°18'N	157°52'W	65	1905–1920 1922–1940 1942–1950	1950–1972
Kahului	20°54'N	156°28'W	19	1951–1960	1965–1975
Hilo	19°44'N	155°4'W	25	0	1949–1974
Wake	19°17'N	166°38'E	16	0	1952–1964 1969–1973
Johnston	16°44'N	169°32'W	19	1953–1961	1967–1978
Guam	13°27'N	144°39'E	22	0	1949–1971
Eniwetok	11°21'N	162°21'E	16	0	1953–1969
Kwajalein	8°44'N	167°44'E	24	0	1953–1964 1965–1978
Truk	7°27'N	151°52'E	20	1952–1954 1956–1958	1960–1974
Majuro	7°10'N	171°5'E	4	0	1968–1972
Fanning	3°54'N	159°24'W	9	1973–1981	0
Christmas	2°0'N	157°30'W	16	1956–1972 1978–1979 1980–1981	0
Canton	2°49'S	171°40'W	22	1949–1967 1977–1980	0
Rabaul	4°12'S	152°11'E	4	1966–1968 1975–1976	0
Anewa Bay	6°13'S	155°38'E	4	1969–1973	0
Apia	13°50'S	171°45'W	13	1954–1962 1967–1971	0
Pago Pago	14°17'S	170°41'W	21	1952–1964	1966–1975
Papeete	17°32'S	149°34'W	6	1969–1974	0
Noumea	22°18'S	166°26'E	13	1967–1979	0
Rikitea	23°8'S	134°57'W	3	1970–1972	0
Easter	27°9'S	109°27'W	5	1957–1958 1970–1971 1974–1975	0

earth) is given to a very good approximation by [e.g., Godin 1972, Eq. (0.28)]

$$\eta_{e,k} = \frac{\Gamma}{g}$$
$$= \frac{G}{g}[0.5A_k(1 - 3\sin^2\theta)\cos(\omega_k t + \alpha_{e,k}) + 1.11803B_k \sin\theta(3 - 5\sin^2\theta') \times \sin(\omega_k t + \alpha_{e,k})], \quad (A.1)$$

where the subscript k refers to a particular tidal constituent, θ (θ') is the latitude (colatitude) of the observer on the earth, $\alpha_{e,k}$ is phase relative to a common start time, the periods $2\pi/\omega_k$ and coefficients A_k and B_k are listed in Table A2 for the largest tides with periods near 1 and 2 cycles per lunar month, and G is proportional to a constant times the radius of the earth at the observer such that $G \approx 26.8$ cm $\times g$.

The actual measured form of the sea level response to the tidal potential Γ is represented in a form that includes a multiplicative constant and phase shift not present in (A.1), such that

$$\eta_k = \nu_k H_k(\theta, \phi)\cos(\omega_k t + \alpha_k + \mu_k), \quad (A.2)$$

where ϕ is longitude, H_k and α_k are the amplitude and phase of the true tide at frequency ω_k, and $\nu_k H_k$ and $(\alpha_k + \mu_k)$ are the amplitude and phase obtained from the Fourier transform at ω_k. The terms ν_k and μ_k arise from the practical constraint that with short (a few years) record lengths it is impossible to resolve tides, by Fourier analysis, which differ in frequency by only 1 cycle per 18.6 years, for instance, such as Mf and its neighbor at Doodson number 075565 in Table A2. These neighboring tidal constituents beat against each other producing years with larger fortnightly tides than others. For example, the fortnightly tide is twice as strong in 1987 as it is in 1978. Practical measurement of the tide is subsequently more difficult in 1978 if the noise level is high. The frequency splitting of the tides that gives rise to the 18.6-year beat is due to the regression of the lunar nodes (e.g., Godin 1972), hence, the name "lunar nodal factors" for ν_k and μ_k. In practice, we estimated ν_k for Mf and Mm semiannually (following Schureman 1958), then averaged for the whole time period of a given data record that was input to the FFT. Hence, if longer (say, 8 year) records are FFT'ed, the averaged nodal factor will reflect the fact that the FFT is beginning to resolve neighboring constituents. The observed amplitudes of the Mf and Mm tides in Tables A3 and A4, respectively, have been corrected with averaged lunar nodal amplitude factors. (Note that the stations in Tables A3 and A4 have been ordered from north to south for ease of comparison with Figs. 1 and 2.)

TABLE A2. Long-period tide coefficients.

Doodson number	Period, $2\pi/\omega_k$ (solar days)	A_k* ($\times 10^{-5}$)	B_k* ($\times 10^{-5}$)	Darwin symbol
063 645	31.961	−113		
063 655	31.812	1 579		
063 665	31.664	−103		
065 445	27.667	−542		
065 455	27.555	8 254		Mm
065 465	27.443	−536		
065 555	27.322		466	
065 655	27.093	−441		
065 665	26.985	−180		
067 455	23.942	−115		
073 555	14.765	1 369		MSf
075 355	13.777	676		
075 555	13.661	15 647		Mf
075 565	13.633	6 483		
075 575	13.606	606		

* Taken from Cartwright and Edden (1973) and Cartwright and Tayler (1971). A blank implies zero.

The nodal amplitude factor ν_k, calculated as just described, incorporates the beating of Doodson numbers 075565 and 075575 with Mf, and Doodson numbers 065445 and 065465 with Mm. For very short records (under two years) fewer of the constituents in Table A2 are resolved from Mf or Mm, suggesting that the nodal factor correction really should incorporate more constituents, a fact that is fully discussed in Godin (1972). Only infrequently are fewer than four years of data analyzed at a time here, so that the additional complication of incorporating other constituents into the nodal factor correction was not considered necessary. The phase nodal factor μ_k is not estimated at all, since the observed phase is given below only in terms of its relation to the equilibrium tide phase, in which case the phase nodal factor cancels out, as will be shown.

A simple measure of the nonequilibrium nature of the tides is obtained from the "driving point admittance" (Wunsch 1967). If the observed and equilibrium tides are represented as complex exponentials such that

$$\eta_k = \nu_k H_k(\theta, \phi)e^{i(\omega_k t + \alpha_k + \mu_k)}, \quad (A.3a)$$

and

$$\eta_{e,k} = \nu_k H_{e,k}(\theta, \phi)e^{i(\omega_k t + \alpha_{e,k} + \mu_k)}, \quad (A.3b)$$

then the admittance at ω_k is defined as

$$Y_k(\theta, \phi) = |Y_k(\theta, \phi)|e^{-i\psi_k} \equiv \frac{\eta_k}{\eta_{e,k}} = \frac{H_k}{H_{e,k}}e^{i(\alpha_k - \alpha_{e,k})}, \quad (A.4)$$

where $|Y_k(\theta, \phi)|$ and ψ_k are the admittance amplitude and phase, respectively. Note that this admittance definition differs from that of Cartwright and Ray (1990) and Ray and Cartwright (1992), who allow their admittance to carry the latitude dependence of the tide.

TABLE A3. Fortnightly tide, Mf.

Station name	Total number of years of data	Observed amp. (cm) $\lvert\eta\rvert$	Equilibrium tide, $\eta_e = \Gamma/g$: Amp. (cm) $\lvert\eta_e\rvert$	Self-consistent correction	Self-consistent amp. (cm) $\lvert\eta_{se}\rvert$	Admittance, η/η_{se}: Amp. $\lvert\eta/\eta_{se}\rvert$	Phase (deg) $<\eta_{se} - <\eta$	Dynamic tide, $\eta - \eta_{se}$: Amp. (cm) $\lvert\eta - \eta_{se}\rvert$	Phase (deg) $<(\eta - \eta_{se})$
Midway	19	.39 ± .15	.66	.71	.47	.85 ± .33	86 ± 22	.59 ± .15	138 ± 15
Nawiliwili	18	.60 ± .11	1.22	.76	.92	.66 ± .12	41 ± 10	.61 ± .11	140 ± 10
Mokuoloe	13	.55 ± .15	1.28	.76	.97	.56 ± .16	30 ± 16	.57 ± .15	151 ± 15
Honolulu	65	.58 ± .05	1.26	.76	.95	.61 ± .05	39 ± 5	.62 ± .05	144 ± 4
Kahului	19	.65 ± .08	1.28	.76	.97	.67 ± .06	46 ± 7	.70 ± .08	138 ± 6
Hilo	25	.67 ± .07	1.36	.77	1.04	.64 ± .06	41 ± 6	.69 ± .07	141 ± 5
Wake	16	.63 ± .14	1.48	.75	1.12	.56 ± .13	36 ± 13	.71 ± .14	149 ± 11
Johnston	19	.94 ± .23	1.61	.77	1.24	.81 ± .18	32 ± 14	.67 ± .23	132 ± 20
Guam	22	.90 ± .09	1.71	.76	1.29	.70 ± .07	14 ± 6	.47 ± .09	153 ± 11
Eniwetok	16	.96 ± .09	1.83	.77	1.42	.68 ± .07	14 ± 5	.54 ± .09	154 ± 10
Kwajalein	24	1.01 ± .05	1.89	.78	1.47	.69 ± .04	16 ± 3	.57 ± .05	151 ± 5
Truk	20	1.12 ± .06	1.99	.76	1.51	.75 ± .04	15 ± 3	.51 ± .06	146 ± 7
Majuro	4	1.16 ± .14	1.99	.78	1.56	.74 ± .09	21 ± 7	.63 ± .14	139 ± 13
Fanning	9	1.15 ± .21	2.00	.78	1.57	.74 ± .14	14 ± 11	.53 ± .21	148 ± 24
Christmas	16	1.29 ± .10	2.05	.78	1.61	.80 ± .06	11 ± 4	.43 ± .10	145 ± 14
Canton	22	1.36 ± .13	2.04	.79	1.61	.84 ± .08	18 ± 5	.48 ± .13	127 ± 15
Rabaul	4	1.19 ± .18	2.12	.76	1.60	.74 ± .11	4 ± 9	.42 ± .18	169 ± 27
Anewa Bay	4	1.01 ± .34	1.98	.76	1.51	.67 ± .23	1 ± 19	.50 ± .34	178 ± 43
Apia*	13	.97 ± .21	1.74	.77	1.33	.73 ± .16	7 ± 12	.38 ± .21	162 ± 34
Pago Pago	21	.92 ± .10	1.77	.77	1.36	.68 ± .07	19 ± 6	.57 ± .10	148 ± 10
Papeete	6	.73 ± .22	1.52	.77	1.17	.62 ± .19	45 ± 17	.83 ± .22	142 ± 15
Noumea	13	.62 ± .34	1.18	.72	.85	.74 ± .40	38 ± 31	.52 ± .34	133 ± 40
Rikitea	3	.86 ± .32	1.12	.74	.83	1.03 ± .39	54 ± 21	.77 ± .32	115 ± 25
Easter	5	.64 ± .50	.82	.76	.62	1.03 ± .80	63 ± 43	.66 ± .50	120 ± 49

* Estimates for Apia are suspect due to anomalously large nonlinear tide at MSf.

TABLE A4. Monthly tide, Mm.

Station name	Total number of years of data	Observed amp. (cm) $\lvert\eta\rvert$	Equilibrium tide, $\eta_e = \Gamma/g$: Amp. (cm) $\lvert\eta_e\rvert$	Self-consistent correction	Self-consistent amp. (cm) $\lvert\eta_{se}\rvert$	Admittance, η/η_{se}: Amp. $\lvert\eta/\eta_{se}\rvert$	Phase (deg) $<\eta_{se} - <\eta$	Dynamic tide, $\eta - \eta_{se}$: Amp. (cm) $\lvert\eta - \eta_{se}\rvert$	Phase (deg) $<(\eta - \eta_{se})$
Midway	19	.18 + .28 − .18	.37	.71	.26	.71 + 1.07 − .71	91 ± 180	.32 ± .28	145 ± 60
Nawiliwili	18	.37 ± .21	.65	.76	.49	.75 ± .42	49 ± 31	.37 ± .21	132 ± 34
Mokuoloe	13	.43 ± .21	.66	.76	.50	.87 ± .42	29 ± 27	.24 ± .21	120 ± 60
Honolulu	65	.43 ± .08	.67	.76	.51	.85 ± .16	16 ± 11	.15 ± .08	128 ± 33
Kahului	19	.45 ± .16	.69	.76	.53	.85 ± .31	24 ± 20	.22 ± .16	123 ± 48
Hilo	25	.62 ± .16	.74	.77	.57	1.10 ± .28	21 ± 14	.22 ± .16	86 ± 44
Wake	16	.50 ± .24	.73	.75	.55	.90 ± .44	15 ± 27	.15 + .24 − .15	119 ± 180
Johnston	19	.30 ± .26	.82	.77	.63	.47 ± .42	50 ± 49	.50 ± .26	153 ± 32
Guam	22	.60 ± .19	.91	.76	.69	.87 ± .28	−9 ± 18	.13 + .19 − .13	45 ± 180
Eniwetok	16	.69 ± .18	.98	.77	.76	.91 ± .24	17 ± 15	.23 ± .18	116 ± 53
Kwajalein	24	.62 ± .10	1.02	.78	.79	.79 ± .12	19 ± 9	.29 ± .10	135 ± 19
Truk	20	.64 ± .12	1.03	.76	.78	.83 ± .16	−1 ± 11	.14 ± .12	5 ± 65
Christmas	16	.72 ± .26	1.11	.78	.87	.83 ± .30	32 ± 21	.46 ± .26	124 ± 35
Canton	22	.84 ± .22	1.09	.79	.86	.98 ± .25	26 ± 15	.38 ± .22	105 ± 35
Apia*	13	1.74 ± .28	.93	.77	.71	2.43 ± .40	16 ± 9	1.07 ± .28	27 ± 15
Pago Pago	21	.55 ± .16	.88	.77	.67	.81 ± .24	18 ± 17	.23 ± .16	132 ± 46
Noumea	13	.47 + .48 − .47	.63	.72	.45	1.03 + 1.05 − 1.03	175 ± 55	.92 + 1.05 − .92	177 ± 180

* Estimates for Apia are suspect (and are not plotted) due to anomalously large nonlinear tide at MSf.

For calculation of the admittance the equilibrium tide is numerically generated, for the same time period and sampling interval as the observed sea level record, from the orbital motions of the earth and moon following the treatment by Munk and Cartwright (1966, appendix A) with updated astronomical constants taken from Harrison (1971). The calculated equilibrium tide time series is analyzed in the same manner as the sea level record, so the resultant Fourier coefficient tide estimates are subject to the same nodal factor corrections as for measured sea level, as indicated by the notation in (A.3b). The admittance (A.4) is then clearly independent of the nodal factor corrections. Also, to lowest order, spurious effects of the transformation process cancel. The magnitude of the equilibrium tide $|\eta_e|$ estimated in this manner at each station is shown in Tables A3 and A4.

For the admittance to truly represent how much the real ocean tides deviate from the *static,* equilibrium limit (where $|Y_k| = 1$ and $\psi_k = 0$), the equilibrium tide just discussed, and the admittance in (A.4) must be adjusted for the static effects of ocean self-attraction and yielding of the earth due to the external potential and change in ocean load, with the real geographical distribution of the ocean taken into account (Agnew and Farrell 1978). The ocean self-attraction and loading factors, etc., were all computed by Agnew and Farrell (1978) assuming the sea level response to the imposed potential is static (mass is conserved). Very roughly, the yielding of the earth due to the external potential reduces the equilibrium tide by about 30%, ocean loading and self-attraction on a completely water-covered earth would increase the tide by about 25%, and consideration of the true distribution of the water mass generally reduces the equilibrium tide by 0%–15% in a spatially dependent manner [thus the longitude dependence explicit in (A.3b)]. Numerical values of the static tide computed by Agnew and Farrell, based on the structure of the long-period tidal forcing represented by the first term in the brackets in (A.1), were generously provided by Agnew (1978, personal communication). These static tide estimates were used to generate amplitude reduction factors (called "self-consistent correction" in Tables A3 and A4) that were applied to the equilibrium tide amplitude $|\eta_e|$ to obtain the self-consistent equilibrium tide amplitude $|\eta_e|$ and subsequently the admittance amplitude from (A.4). The phase of η_{se} equals the phase of η_e, so that the admittance phase ψ_k is unaffected by the self-consistent correction. A positive admittance phase in Tables A3 and A4 and Figs. 1 and 2, indicates that sea level lags behind the equilibrium tide.

The most critical problem in estimating the amplitudes of the long-period tides is contamination by "noise," or rather, the background continuum level of energy around the tidal frequencies. The continuum level is generally related to atmospheric forcing away from strong boundary current regions (especially, due to sea level's static response to surface air pressure fluctuations), is a strong function of frequency, rising with increasing period, and is a strong function of position, in accordance with geographical changes in the atmospheric forcing and oceanic response. The tides are deterministic signals so the stochastic noise contaminating the Fourier transform tide estimates can be reduced by increasing the record length (e.g., Wunsch 1967). In practice, very long, continuous records are rare, especially in the Pacific. Four- and eight-year record lengths were found to be adequate for reducing the noise level, while providing excellent alignment characteristics.

Alignment of the tidal line on a Fourier harmonic is almost as important as noise in estimating H_k and the admittance. If the frequency of a tidal line falls between the harmonics of the Fourier transform, that tide's energy is divided among the neighboring Fourier harmonics, reducing the estimated amplitude of the tide (from the nearest harmonic). Since the equilibrium tide time series is analyzed in a manner equivalent to the sea level data, to lowest order the effect of the transform misalignment is canceled out in the computation of the admittance, with one important caveat. If the tidal line is already weak, the misalignment increases the effect of noise and the accuracy of the resultant admittance estimate is substantially reduced. Alignment error, unlike noise error, is not a function of record length. The analyses completed here always aligned the tide under consideration so that the expected error from misalignment is less than 2%. The record lengths of 1462 solar days and 2923 solar days deserve special mention not only for their alignment of Mf and Mm, but for their excellent alignment of almost all of the major diurnal and semidiurnal tidal constituents. For those tide pairs separated by only 1 cycle per 18.6 years (such as Mf and Doodson number 075565 in Table A2), the larger component was aligned, although an argument can be made for locating the Fourier harmonic between the two tides.

Confidence intervals are essential to the interpretation of the estimates of tidal amplitude, phase, and admittance. Assuming the noise has approximately a normal probability distribution and has constant variance in a small frequency band containing the tidal line under consideration, then the probability distributions for $|\eta_k|$, $|Y_k|$, and ψ_k, and so on, are readily determined following the analysis of Munk and Cartwright (1966, appendix B) modified by us to include the uncertainty in the estimate of the noise variance around the tidal line. The noise variance was taken to be an average of the variance at 6 to 12 Fourier harmonics surrounding the constituent under consideration but outside the frequency band where the forcing was significant (see Table A2). Tables A3 and A4 and Figs. 1 and 2 display the 90% confidence intervals es-

timated as described here. Finally, the tide amplitudes $|\eta_k|$, and consequently the admittance amplitudes $|Y_k|$, have been corrected for a small bias due to the noise variance (Wunsch 1967).

For any given station, data was often available from several different decades, but usually the data had significant gaps. Consequently, tide estimates were made using pieces of data (typically, with lengths of 1462 or 2923 days) that then were combined with appropriate scalar or vector averaging (weighted by the number of years of data per estimate) to achieve the final estimates shown in Tables A3 and A4 and Figs. 1 and 2. It was found that at least 3 (10) years of data were needed to obtain amplitude estimates of Mf (Mm) that had any meaningful statistical significance, hence the smaller number of stations listed in Table A4 than Table A3. The dynamic tide $\eta - \eta_{se}$ and its confidence limits shown in Tables A3 and A4 are straightforward derivations from the estimates and confidence limits previously discussed.

It is well known that hydrodynamical nonlinearities may produce large tidal fluctuations at the sum and difference frequencies of two or more of the strong diurnal and semidiurnal tides. Since several of the difference frequencies exactly equal the frequencies of the long-period tides studied here, it is necessary to investigate the possibility that the observed long-period tides are actually due to nonlinear tides. The strongest nonlinear long-period tide is theoretically the tide due to the interaction of the strongest daily tides, usually the semidiurnal M_2 and S_2, which have a difference frequency exactly equal to the weak linear long-period tide with Doodson number 073555 (MSf in Table A2). Each linear tide in Table A2 corresponds to the difference frequency of at least one pair of daily tides that are weaker than M_2 and S_2, so if the observed MSf tide is not strongly different from its equilibrium value we may conclude that the rest of the nonlinear long-period tides are small. The MSf tide has been sought at all the stations listed in Table A1. Only at Apia was an anomalously large (up to 30 times equilibrium) MSf tide observed. Consequently, the large Mm tide from Apia listed in Table A4 is considered the result of nonlinear contamination and is not plotted; the Mf tide from Apia appears normal but is suspect.

APPENDIX B

Finite-Element Linear Shallow-Water Time-Stepping Model

Following the finite-element formulation and numerical manipulation designed by Platzman (1978) for the linearized shallow-water equations, we constructed an explicit time-stepping version of (3.1) that is flexible in choice of geometry, topography, and resolution on the sphere. After rewriting (3.1) in terms of a velocity potential ϕ and streamfunction ψ and expanding in a linear finite-element basis, (3.1) becomes in matrix notation

$$\mathbf{B}\mathbf{X}_t = (\mathbf{A} - \mathbf{D})\mathbf{X} + \mathbf{a}, \tag{A.1}$$

where $\mathbf{X}$ is the vector of expansion coefficients for the finite-element expansion of (η, ψ, ϕ). The matrices $\mathbf{B}$ and $\mathbf{A}$ correspond, respectively, to symmetric and skew-symmetric operator matrices derivable from (3.1), while the vector $\mathbf{a}$ is the residual term associated with the incompleteness of any finite-element basis. The dissipation matrix $\mathbf{D}$ has been coded to include the effect of only linear bottom drag, the coefficient of which may be proportional to any power of the ocean depth.

The time-stepping procedure is as follows: First the factorization of $\mathbf{B} = \mathbf{C}\mathbf{C}^{\mathrm{T}}$ is computed (one time only). Then we define $\mathbf{Y} = \mathbf{C}^{\mathrm{T}}\mathbf{X}$, so that

$$\mathbf{C}\mathbf{Y}_t = (\mathbf{A} - \mathbf{D})\mathbf{X} + \mathbf{a}. \tag{A.2}$$

After specifying an initial condition $\mathbf{Y}_0 = \mathbf{C}^{\mathrm{T}}\mathbf{X}_0$, $\mathbf{Y}_t$ is obtained by forward substitution. The new $\mathbf{Y}$ is computed by leapfrog and the new $\mathbf{X}$ is then computed by backward substitution.

We first tested the time-stepping code with neither damping nor forcing. These tests revealed that an arbitrary initial condition conserved the total energy to within approximately 1%, depending on the size of the time step. Second, if the code was initialized with a normal-mode solution, computed following Platzman (1978), the evolving solution conserved energy (to within 1%), oscillated at nearly the computed free period, and maintained its spatial integrity.

We next tested the code with no forcing but with constant bottom friction coefficient r. From the shallow-water energy equation, we expect that total energy will decrease according to the (mode dependent) formula

$$\frac{\partial}{\partial t}(E_1 + E_2) = -2rE_2, \tag{A.3}$$

where

$$E_1 = \iint_{\text{basin}} \tfrac{1}{2} g\eta^2 dxdy, \tag{A.4}$$

$$E_2 = \iint_{\text{basin}} \tfrac{1}{2} h^{-1}(u^2 + v^2) dxdy. \tag{A.5}$$

For a single normal mode over one wave period, we can rewrite (A.3) as

$$\frac{\partial}{\partial t} E = -2r(1 - \alpha)E, \tag{A.6}$$

where $E_1 = \alpha E$, $E_2 = (1 - \alpha)E$, and $E = E_1 + E_2$. The values for E_1 and E_2 are easily computed from the

normal-mode solutions. Gravity normal modes, being nearly equipartitioned in energy, have $\alpha_g \approx 0.45$, while planetary–topographic modes, with nearly all their energy in the rotational velocity field, have $\alpha_p \approx 0.05$. For several cases of a normal mode as initial condition with constant damping, we found (A.4) to be accurate to within 1%.

When leapfrog time stepping was used in tests with both tidal forcing and dissipation, the well-known 2-δx waves (e.g., Gray and Lynch 1977; Kinnmark and Gray 1985) became evident and eventually they dominated the solution, particularly near certain points of the boundaries. The source for the excitation of the 2-δx waves became readily evident by solving a one-dimensional finite-element shallow-water problem. We found that, although the physical mode is damped at the normal rate, the computational mode is forced, rather than damped, by the linear bottom drag. The rate of excitation of the computational mode by bottom drag increases with decreasing length scale (and, hence, increasing frequency for gravity waves). The question of why the 2-δx waves near the boundaries were excited the most strongly was answered by referring to the significant paper of Platzman (1981). Platzman showed that inhomogeneous triangulation can lead to an abnormal branch of the dispersion curve for two-dimensional waves. Since the boundaries of our domain are necessarily inhomogeneously triangulated, Platzman's results suggest that, for the finite-element formulation here, high-frequency abnormal waves can exist in the regions of the boundary where inhomogeneous triangulation occurs. Since the nodes of the boundary are often displaced to conform to observed boundaries, the distance between boundary nodes is smaller in some places than in others. Hence, the reason that the boundary locations correspond to strongest excitation of the 2-δx waves is because the computational mode associated with the abnormal wave there is preferentially excited for the smallest spatial scales, namely, the grid scale. Since the 2-δx noise was computational (due to centered differencing), we easily suppressed it by using Euler backward time stepping. We then found that a weak (amplitude 0.02) Robert–Asselin time filter (Asselin 1972) effectively extinguished the computational modes, and was nearly as cost efficient and energy conserving as the leapfrog time step. The abnormal waves are relatively small scale, boundary trapped, and high frequency and thus will not offend our low-frequency solutions.

The code was then further tested by including short-period forcing with period very close to a known (i.e., computed) gravitational mode. The gravity-mode structure clearly appeared in the response. Next we compared weakly damped time-stepping results with solutions obtained from modal syntheses (following Platzman 1984) and found the solutions to be very similar. Lastly, we examined strongly damped time-stepping results with the solutions obtained from modal reconstructions with strong damping. As expected, the results were significantly different due to the expansion in terms of inviscid or perturbatively viscid modes.

All solutions discussed in the text were forced by an equilibrium tide with the basin mean removed. The subjective criteria for convergence of solutions from cycle to cycle were visual similarity of solutions and the basinwide energy diagnostics. To encourage more rapid convergence of the weakly damped solutions, we incrementally decreased the damping coefficient from strong values at the commencement of the run to the desired value for the final few cycles.

REFERENCES

Agnew, D. C., and W. E. Farrell, 1978: Self-consistent equilibrium ocean tides. *Geophys. J. R. Astron. Soc.*, **55,** 171–181.

Asselin, R. A., 1972: Frequency filter for time integrations. *Mon. Wea. Rev.*, **100,** 487–490.

Carton, J. A., 1983: The variation with frequency of the long-period tides. *J. Geophys. Res.*, **88,** 7563–7571.

Cartwright, D. E., and R. J. Tayler, 1971: New computations of the tide-generating potential. *Geophys. J. R. Astron. Soc.*, **23,** 45–74.

——, and A. C. Edden, 1973: Corrected tables of tidal harmonics. *Geophys. J. R. Astron. Soc.*, **33,** 253–264.

——, and R. D. Ray, 1990: Observations of the Mf ocean tide from Geosat altimetry. *Geophys. Res. Lett.*, **17,** 619–622.

Darwin, G., 1886: On the dynamical theory of the tides of long period. *Proc. Roy. Soc. London, Ser. A,* **41,** 319–336.

Davey, M. K., W. H. Hsieh, and R. C. Wajsowicz, 1983: The free Kelvin wave with lateral and vertical viscosity. *J. Phys. Oceanogr.*, **13,** 2182–2191.

Davis, R. E., and P. S. Bogden, 1989: Variability on the California Shelf forced by local and remote winds during the Coastal Ocean Dynamics Experiment. *J. Phys. Oceanogr.*, **94,** 4763–4783.

Dickman, S. R., 1989: A complete spherical harmonic approach to luni-solar tides. *Geophys. J. Int.*, **99,** 457–468.

Godin, G., 1972: *The Analysis of Tides.* University of Toronto Press, Toronto, Canada, 264 pp.

Gray, W. G., and D. R. Lynch, 1977: Time-stepping schemes for finite element tidal model computations. *Adv. Water Resour.*, **1,** 83–95.

Harrison, J. C., 1971: New computer programs for the calculation of earth tides. Unpublished manuscript.

Hendershott, M. C., 1981: Long waves and ocean tides. *Evolution of Physical Oceanography,* C. Wunsch and B. Warren, Eds., The MIT Press, 292–341 pp.

Hough, S. S., 1897: On the application of harmonic analysis to the dynamical theory of the tide, 1. *Philos. Trans. Roy. Soc. London, Ser. A,* **189,** 201–257.

Kagan, B. A., V. Y. Rivkind, and P. K. Chernyayev, 1976: The fortnightly lunar tides in the global ocean. *Izv. Acad. Sci. USSR, Atmos. Oceanic Phys.*, **12,** 274–276.

Kinnmark, I. P. E., and W. G. Gray, 1985: The 2δx-test: A tool for analyzing spurious oscillations. *Adv. Water Resour.*, **8,** 129–135.

Lamb, H., 1932: *Hydrodynamics.* 6th ed. Dover, 738 pp.

Laplace, P. S., 1775: Recherches sur quelques points du systeme du monde. *Mem. Acad. Roy. Soc.*, 75–182.

Levitus, S., 1982: *Climatological Atlas of the World Ocean.* NOAA Prof. Paper 13, U.S. Govt. Printing Office, Washington, D.C., 173 pp.

Luther, D. S., 1980: Observations of long period waves in the tropical oceans and atmosphere. Ph.D. dissertation. Joint Program in Oceanography, Massachusetts Institute of Technology and the Woods Hole Oceanographic Institution, 210 pp.

Miles, J. W., 1974: On Laplace's tidal equations. *J. Fluid Mech.*, **66,** 241–260.

Miller, A. J., 1986: Barotropic planetary-topographic oscillations in ocean basins. Ph.D. dissertation. University of California, San Diego, 133 pp.

——, 1992: On forced barotropic vorticity oscillations. *J. Phys. Oceanogr.*, **22,** 808–810.

Mofjeld, H. O., 1980: Effects of vertical viscosity on Kelvin waves. *J. Phys. Oceanogr.*, **10,** 1039–1050.

Munk, W. H., and D. E. Cartwright, 1966: Tidal spectroscopy and prediction. *Phil. Trans. Roy. Soc. London,* **A259,** 533–581.

Platzman, G. W., 1978: Normal modes of the world ocean. Part I: Design of a finite-element barotropic model. *J. Phys. Oceanogr.*, **8,** 323–343.

——, 1981: Some response characteristics of finite-element tidal models. *J. Comput. Phys.*, **40,** 36–63.

——, 1984: Normal modes of the world ocean. Part III: A procedure for tidal synthesis. *J. Phys. Oceanogr.*, **14,** 1521–1531.

Ponte, R. M., D. A. Salstein, and R. D. Rosen, 1991: Sea level response to pressure forcing in a barotropic numerical model. *J. Phys. Oceanogr.*, **21,** 1043–1057.

Proudman, J., 1913: Limiting forms of long period tides. *Proc. London Math. Soc.*, Ser. 2, **13,** 273–306.

Ray, R. D., and D. E. Cartwright, 1992: Satellite altimeter observations of the Mf and Mm ocean tides, with simultaneous orbit corrections. *Proc. XX General Assembly, Int. Union Geod. Geophys.*, Vienna, Austria, 1991.

Schureman, P., 1958: *Manual of Harmonic Analysis and Prediction of Tides.* U.S. Coast and Geodetic Survey Spec. Publ. No. 98 [revised 1940 ed. reprinted with corrections], U.S. Govt. Printing Office, Washington, D.C.

Schwiderski, E. W., 1982: Global ocean tides, 10, the fortnightly lunar tide (Mf). *Atlas of Tidal Charts and Maps,* Rep. TR 82-151, Naval Surface Weapons Center, Dahlgren, Virginia.

Wunsch, C., 1967: The long-period tides. *Rev. Geophys. Space Phys.*, **5,** 447–475.